JOURNAL OF CATALYSIS 132, 275–286 (1991)

Adsorption of NO and CO on $Rh/ZrO_2(100)$

G. S. ZAFIRIS AND R. J. GORTE

Department of Chemical Engineering, University of Pennsylvania, Philadelphia, Pennsylvania 19104

Received May 24, 1991; revised July 25, 1991

The structure and adsorption properties of Rh films supported on a $ZrO_2(100)$ crystal have been examined using Auger electron spectroscopy (AES), transmission electron microscopy (TEM), and temperature programmed desorption (TPD) of NO and CO. For Rh vapor deposition at 300 K, film growth is close to two dimensional; however, metal particles are formed by heating above ~500 K or exposure to air. Transmission electron diffraction (TED) indicates that the particles are preferentially oriented with respect to the substrate, which implies that interactions exist between the support and the Rh. TPD curves for CO are essentially independent of particle size and are similar to curves obtained on bulk Rh crystals. However, TPD curves for NO are strongly affected by particle size and film annealing. For particles between 3 and 10 nm formed by annealing, more than 98% of the NO dissociated during TPD from a saturation exposure. For the 10-nm particles, the TPD results were similar to curves on bulk metals in that N_2 left the surface from two separate features: a sharp peak at 440 K due to $NO_{ad} + N_{ad} = N_2 + O_{ad}$ and a broad feature between 450 and 700 K due to N_{ad} recombination. For smaller particles, only the recombination feature was observed at approximately the same temperature. The implications of these results to understanding support and particle size effects for NO reduction by CO are discussed. The results do not indicate strong electronic interactions between Rh and ZrO_2, but do suggest that Rh particle morphologies may be altered by ZrO_2, which could, in turn, affect catalytic properties.

INTRODUCTION

The effect of the support on the performance of a metal catalyst can be very important. This is especially true for automotive emission-control catalysts, for which the choice of support can change both the activity and the stability. For example, the activity of $Rh/CeO_2/Al_2O_3$ for NO reduction by CO at low temperatures is higher than that of Rh/Al_2O_3 (*1*), and the stability of Rh/ZrO_2 catalysts is reported to be considerably better than that of Rh/Al_2O_3 (*2*). The interactions between the support and the metal which lead to these variations in catalyst activity and stability are not well understood at the present time. Providing a better understanding of these interactions was the motive of this study.

We have chosen to study NO and CO adsorption on Rh/ZrO_2 catalysts because of the practical importance of this system and because it appears to be possible to relate the elementary steps in NO reduction by CO, measured in UHV experiments, to actual reaction rates (*3*). A nonporous, model catalyst was examined so that standard surface analysis techniques, like Auger electron spectroscopy (AES), could be applied and in order to simplify the interpretation of the temperature programmed desorption (TPD) results. On high-surface-area samples, TPD results are significantly affected by readsorption and diffusion (*4, 5*). The use of a flat, single-crystal substrate also simplifies the use of transmission electron microscopy (TEM) and allows the structure and orientation of the metal particles with respect to the oxide substrate to be determined using transmission electron diffraction (TED) (*6, 7*).

Previous studies of NO and CO adsorption on $Rh/\alpha\text{-}Al_2O_3(0001)$ suggested that Rh particles interact very weakly with an $\alpha\text{-}Al_2O_3(0001)$ surface (*8, 9*). Rh grew as three-dimensional particles for deposition at 300 K, and TPD curves for CO were essentially identical to curves for bulk Rh. The

0021-9517/91 $3.00

NO desorption results were significantly different from TPD curves found on bulk metals, but this appears to be related to particle size and not to support effects (*10*). Interestingly, changes in the TPD curves with particle size on the model Rh/α-Al_2O_3(0001) catalyst seem to explain the structure sensitivity observed with normal catalysts well (*3, 10, 23*). The TPD results showed that, for very small particles, a low-temperature, N_2 desorption feature due to the reaction $NO_{ad} + N_{ad} = N_2 + O_{ad}$ is eliminated and the recombination N_2 desorption feature is shifted to slightly higher temperatures (*8*). These changes probably lead to higher coverages of atomic nitrogen, which blocks the surface from adsorbing reactants. This could explain why reaction rates are much higher on larger Rh particles (*10*).

In this paper, we shall demonstrate that Rh appears to interact more strongly with ZrO_2(100) than it does with α-Al_2O_3(0001). For vapor deposition at 300 K, the Rh film growth is close to two dimensional, and TED indicates that there is some ordering of the Rh with respect to the substrate. The TPD results for both NO and CO from Rh/ZrO_2(100) and from Rh/α-Al_2O_3(0001) are similar after metal particles are formed; however, annealing conditions did affect the desorption of NO on Rh/ZrO_2, even for multilayer coverages of Rh. This may indicate that the support can affect particle shape, which in turn could change catalytic properties.

EXPERIMENTAL

The experiments were performed in a UHV chamber, which has been described previously (*6*). The chamber has a base pressure of $\sim 2 \times 10^{-10}$ Torr and is equipped with a cylindrical mirror analyzer for AES, a Rh source, a calibrated film-thickness monitor, an ion gun for sample cleaning, and a quadrupole mass spectrometer for TPD. The mass spectrometer is mounted inside a stainless-steel cone with an aperture which allows directed desorption from the crystal in order to minimize lead effects. A ZrO_2(100) crystal, $7 \times 7 \times 1$ mm, was mounted on a Ta foil which could be resistively heated. The temperature of the crystal was measured with a chromel-alumel thermocouple attached to the back side using a UHV-compatible, ceramic adhesive.

The crystal was initially cleaned by ion bombardment, heated to ~770 K in 10^{-7} Torr O_2 for 15 min, and then annealed in vacuum at 770 K for 30 min. Rh was deposited onto the ZrO_2 crystal at 300 K without introducing any impurities detectable by AES. Adsorption was carried out immediately upon deposition and after the Rh layer was heated to various temperatures to induce particle formation. All TPD measurements were carried out with a heating rate of ~6K/sec, and labeled ^{15}NO was used for all NO adsorption measurements. Following TPD runs with NO, the sample was heated to 770 K in 5×10^{-8} Torr H_2 to remove chemisorbed oxygen. Particle sizes for Rh were estimated from the amounts of metal deposited and the CO adsorption capacity, assuming spherical particles. These estimates were later verified by TEM for a metal coverage of 2×10^{15}/cm^2.

Most TEM experiments were performed on a Philips EM 400T with an accelerating voltage of 120 kV, although one high-resolution experiment was performed on a JEOL 4000EX. ZrO_2(100) crystals, 2 mm in diameter and 0.2 mm thick, were first thinned by mechanical grinding and polishing, after which they were dimpled to a thickness of ~20 μm. The crystals were then ion milled at 78 K to perforation. After the samples were checked in the microscope, they were placed in the same UHV chamber used in the TPD measurements, cleaned using the procedures described above, and exposed to $\sim 2.3 \times 10^{15}$Rh/cm^2. The samples were then carried in air to the microscope.

RESULTS

Film Growth

Both AES and TEM were used to monitor the growth of Rh on ZrO_2(100). In Fig. 1 the normalized AES peak intensities for Rh(302

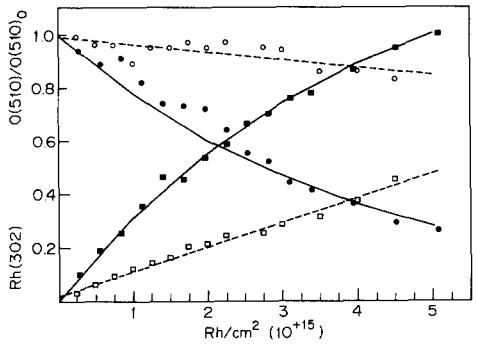

FIG. 1. AES intensities for the Rh(302 eV) and O(510 eV) peaks plotted as a function of metal exposure at 300 K. The filled circles and squares are for ZrO_2(100), while the open points are for α-Al_2O_3(0001). The solid lines are calculated intensities assuming layer-by-layer growth with an electron mean free path of 1.06 nm.

eV) and O(510 eV) are shown as a function of the Rh coverage following deposition on ZrO_2(100) at 300 K, along with previous results for similar experiments on α-Al_2O_3(0001) (*9*). The coverages of Rh were determined from the metal fluxes measured by the film thickness monitor, which had been calibrated in previous experiments (*6*). The intensities of the Rh(302 eV) peak are arbitrary but are on the same scale for both oxide substrates. The intensities of the O(510 eV) peak were normalized to the peak heights of the clean oxide surfaces. It is clear that the growth of Rh on ZrO_2(100) is very different from the growth of Rh on α-Al_2O_3(0001). The O(510 eV) peak decreases much more rapidly with Rh coverage on ZrO_2(100) than on α-Al_2O_3(0001), and the Rh(302 eV) intensity increases much more rapidly. This is consistent with the formation of three-dimensional particles on α-Al_2O_3(0001) and more two-dimensional films on ZrO_2(100).

There is also reasonable agreement between the data for ZrO_2(100) and the model for layer-by-layer growth, shown by the solid line. For this calculation, we assumed that the density of the Rh film is the same as that of bulk Rh and that there are 1×10^{15} Rh/cm^2 in a monolayer. The data was then fit with a mean-free path of 1.06 nm for the O(510 eV) electrons, which is only slightly larger than the expected value of ~0.7 nm for electrons of this energy (*11*). Previous work with Pt on ZrO_2(100) also indicated that Pt growth was almost two-dimensional (*7*). In that work the investigators also found the mean-free path to be slightly larger than expected, and they suggested that the Pt film was not perfectly two-dimensional but contained many defects or gaps. This appears to be true for Rh films as well.

The effect of the initial heating of the Rh film in vacuum is shown in Fig. 2 for a coverage of $\sim 5.7 \times 10^{15}$Rh/cm^2. The data in this figure was obtained by heating the sample to the indicated temperature for 1 min, cooling it to room temperature, and taking the spectrum. Above approximately 450 K, there is a significant and irreversible decrease in the intensity of the Rh(302 eV) peak and an increase in the O(510 eV) peak. These results are again similar to those for Pt on ZrO_2(100) and are indicative of particle formation of a two-dimensional film (*7*). The data in Fig. 2 would also be consistent with migration of Rh into the zirconia; however, the TEM results to be discussed shortly provide no evidence for this. It should be noted that Rh films on α-Al_2O_3(0001), for which particle formation occurs during deposition,

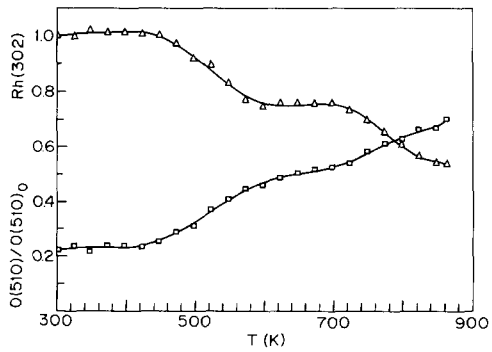

FIG. 2. Plot of the AES peak intensities for 5.7×10^{15}Rh/cm^2 on ZrO_2(100) as a function of temperature after deposition at 300 K. The decrease in the Rh(302 eV) intensity and increase in the O(510 eV) were irreversible.

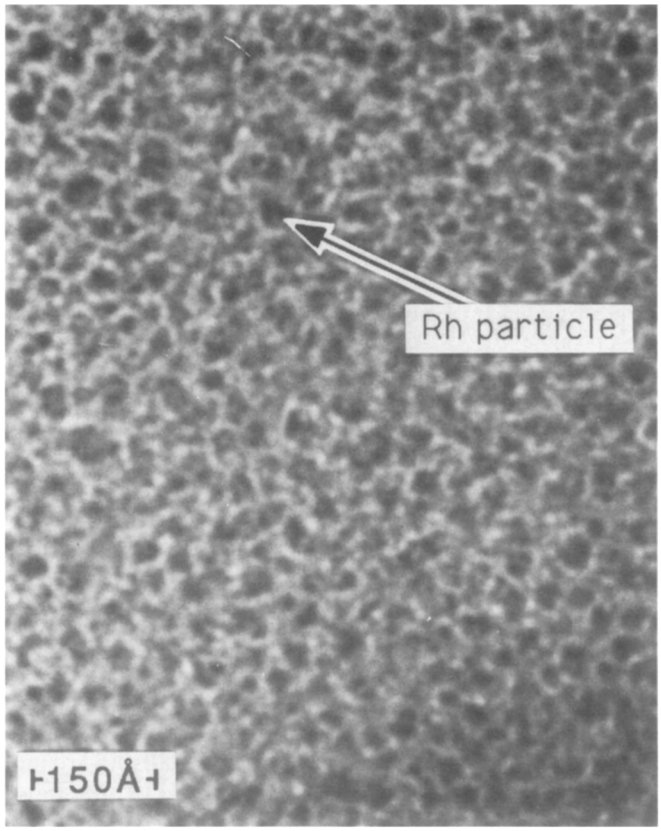

FIG. 3. Bright field image following deposition 2.3 $\times$ 10^{15} Rh/cm^2 on ZrO_2(100) at 300 K.

do not show similar changes in the AES intensities with heating (*19*).

TEM was also used to study the growth of Rh on ZrO_2(100). Figure 3 shows the bright field image following deposition of 2.3 $\times$ 10^{15}Rh/cm^2 at 300 K and indicates that the Rh exists as closely spaced islands, ~2.0–2.5 nm in diameter. While the amount of Rh present in the islands is in reasonable agreement with the amount of Rh originally deposited on the sample, assuming that the islands are as high as they are wide, the fraction of the surface that is uncovered by Rh is larger than would be expected from the attenuation of the O(510 eV) peak in AES at this coverage. We suggest that exposure of the sample to the air may have caused changes in the film, resulting in the formation of larger metal particles. This has been observed previously for Pt on ZrO_2(100).

At higher magnification, moire fringes, which are due to the different lattice spacings of Rh and ZrO_2, can be observed on many of the particles in Fig. 4. The frequency of these fringes varies from particle to particle, indicating that the particles have differing orientations with respect to the [100] zone axis of ZrO_2. However, there does appear to be some ordering of the particles, which can be seen more easily in the TED pattern in Fig. 5. The bright spots in the square array are due to the ZrO_2(100) crystal tilted to the [100] zone axis. With the introduction of Rh, the dashed ring appears. The ring shows arcs of increased intensity at 12 positions which correspond to the Rh{220} reflections. The lattice parameter

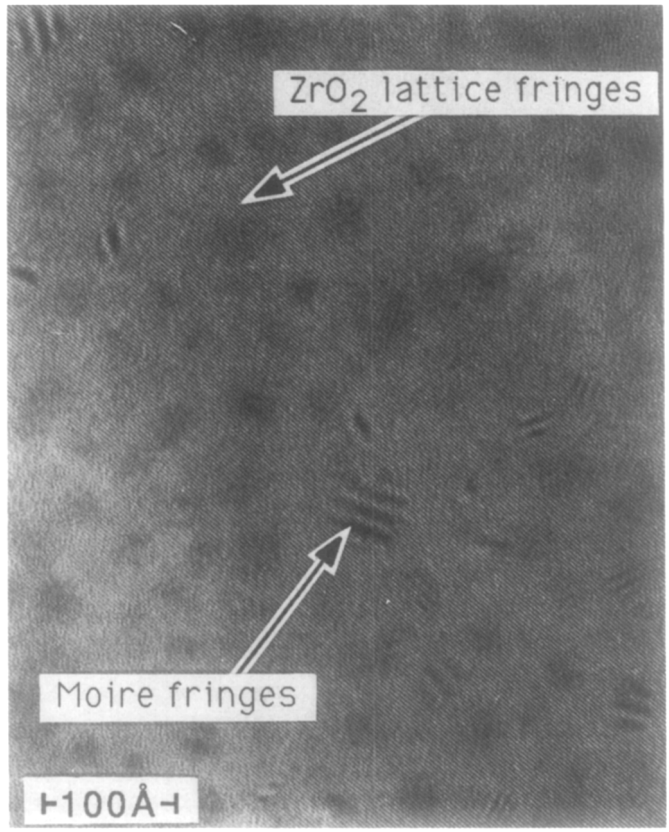

FIG. 4. Bright field image of the same sample as in Fig. 3 at higher magnification.

for Rh, calculated from the position of the ring, is close to the bulk value (±5%). The 12 maxima in the ring can be separated into 2 hexagons, each rotated 30 degrees with respect to each other. Since a Rh single crystal oriented on the [111] zone axis should contain 6 hexagonally arranged, {220} reflections, the Rh must be preferentially oriented to 2 equivalent directions which give rise to these 12 maxima. This result is essentially identical to that obtained for Pt on the ZrO_2(100) surface (*7*), although the maxima with Rh are more diffuse than those observed with Pt.

The effect of annealing the overlayer was also examined by heating the sample in vacuum to 850 K for 2 min, with the resulting bright-field image presented in Fig. 6. The image shows that the Rh islands have formed larger particles with an average particle size of ~3.6–4.0 nm. However, the particles remain oriented with respect to the substrate. The diffraction pattern corresponding to this surface is identical to the one shown in Fig. 5.

TPD of CO

To determine the effect of zirconia on Rh, we first examined the adsorption of CO using TPD. The results for two metal coverages, 5.7×10^{15} Rh/cm^2 and 0.28×10^{15}Rh/cm^2, are shown in Figs. 7(a) and 7(b). These metal coverages were chosen because they represent a large (>5 monolayers) and small (<1 monolayer) coverage of Rh. Figure 7(a) shows the curves obtained immediately after deposition of Rh at 300 K, conditions which result in an almost two-dimensional

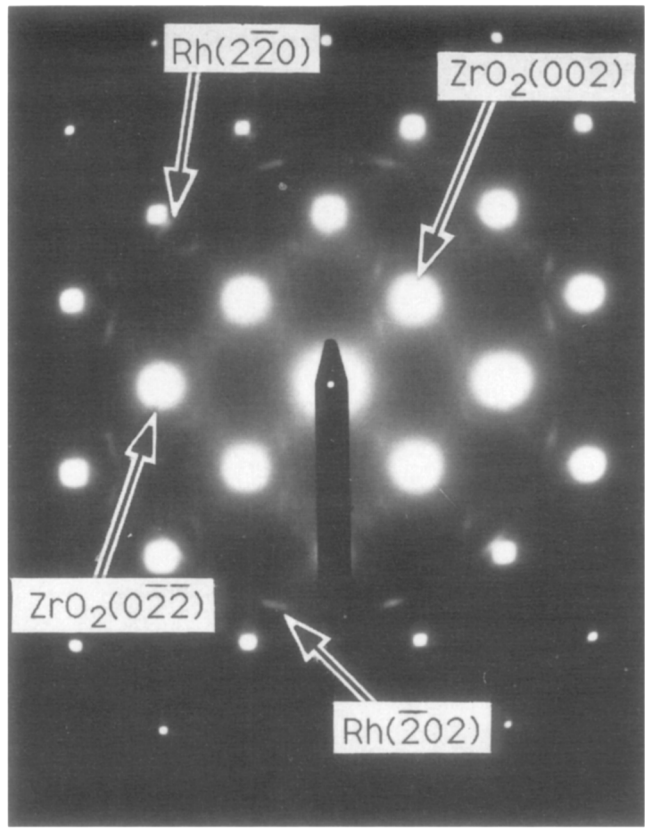

FIG. 5. Transmission electron diffraction obtained following deposition of 2.3 × 10^{15}Rh/cm^2 on ZrO_2(100) at 300 K.

film. Figure 7(b) shows TPD curves obtained from the same surfaces after they had been heated above 800 K in order to form Rh particles. The size of these particles was estimated from adsorption capacities and metal coverages to be approximately 10 nm and 3 nm, respectively. For the larger metal coverage, the shape of the TPD curve is essentially unchanged by heating and is identical to that reported for single crystals and bulk Rh (*12–15*). The main desorption peak is centered at ~480 K, with a shoulder to lower temperatures which may indicate a second peak near 400 K. For the lower metal coverage, the 400-K feature is larger than the peak at 480 K, although the 480-K peak again becomes larger after the Rh layer is annealed. For both large and small particles, the desorption features grow sequentially with increasing CO exposure, as shown in Fig. 7(b).

These TPD results are essentially identical to those obtained in an earlier study of Rh supported on α-Al_2O_3(0001) (*9*). That study also reported only small changes in the CO TPD curves with particle size and showed a relative increase in the intensity of the lower temperature desorption feature on smaller Rh particles. The results in that study were interpreted as indicating that Rh particle size only weakly influences CO adsorption. This is consistent with the observation from single-crystal studies that the crystallographic surface does not affect the desorption of CO from Rh. The small changes observed for very small particles

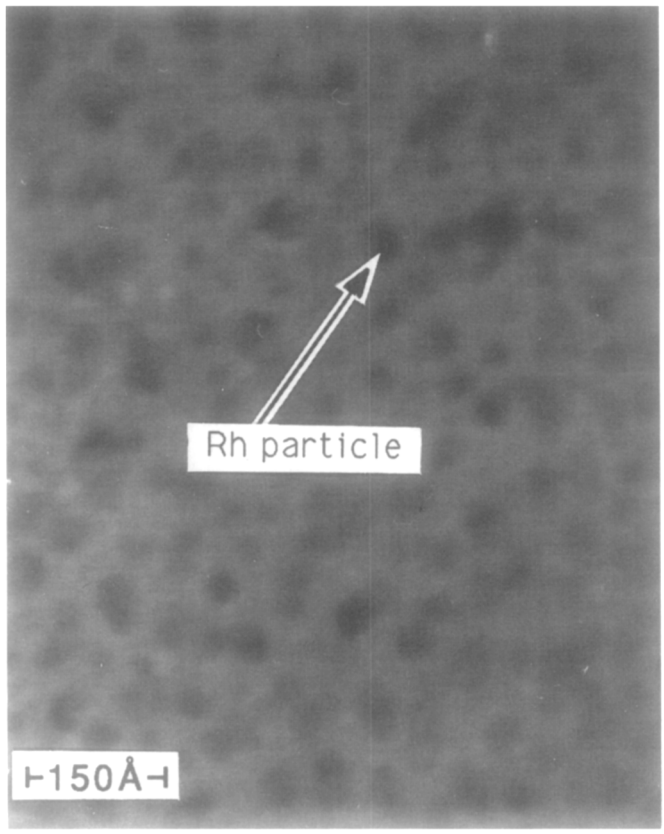

FIG. 6. Bright field image after annealing the sample in Fig. 3 to 800 K.

could be related to the increased adsorption stoichiometry which has been reported for small particles of Rh (*19*); however, the general conclusion is that adsorption bonds do not appear to be strongly affected by particle size or crystallographic surface. The results of our present study suggest that the presence of $ZrO_2(100)$ also had little influence on the adsorption properties of Rh for CO, even for low Rh coverages for which most of the Rh is in contact with $ZrO_2(100)$.

TPD of NO

The adsorption of NO on Rh, as measured by TPD, has been shown to be dependent on particle size and crystallographic surface (*8, 12, 13, 16, 17*). This makes it difficult to separate support effects from morphological effects, since changes in the TPD curves could also be due to particle shape or particle size. However, the similarity between the TPD curves for NO reported in this paper and those obtained previously for Rh on α-$Al_2O_3(0001)$ (*8*) suggest that ZrO_2 did not radically change the adsorption properties of Rh.

We first examined TPD curves from surfaces which had been annealed prior to adsorption in order to form three-dimensional particles. The results for three particle sizes are shown in Fig. 8. Since oxygen could not be removed thermally in our experiments, only the peaks at $m/e = 31$ (^{15}NO) and $m/e = 30$ ($^{15}N_2$) are shown. For the largest particles, the TPD curve is very similar to that observed for Rh single crystals, with the exception that a larger fraction of the NO dissociates. The molecular NO desorbs at

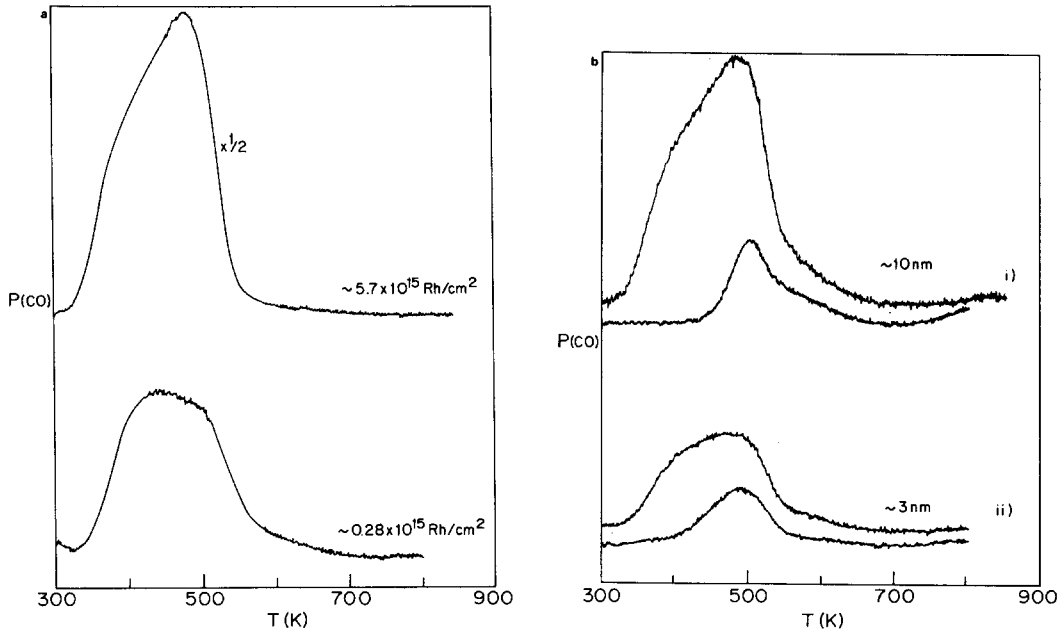

FIG. 7. TPD curves for CO at saturation exposures (a) for unannealed Rh films on $ZrO_2(100)$ and (b) for Rh films after annealing to 800 K. The particle sizes shown in (b) were calculated from dispersion measurements, and the smaller curves were obtained following a lower exposure to CO.

the same temperature, ~430K; but, assuming equal sensitivities for N_2 and NO, approximately 98% of the NO dissociates on the 10-nm particles compared to 55% on Rh(111) (*12*). The N_2 desorbs from two well-defined features which are also observed on Rh(111). The first, a sharp peak at ~440 K, has been identified on several Rh crystals as being due to the reaction $NO_{ad} + N_{ad} = N_2 + O_{ad}$. The second broad feature between 450 and 700 K has been assigned to the recombination of dissociatively adsorbed nitrogen. The temperature for this process is dependent on crystallographic surface, with the peak temperature occurring at ~700 K on Rh(100) compared to ~550 K on Rh(111) and Rh(110) (*12, 13,16, 17*). On the Rh particles, the recombination peak is broad and may indicate a range of different types of desorption states. For the smaller Rh particles, all of the NO dissociates and the 440-K, N_2 desorption feature disappears. Only the recombination N_2 feature is observed. This feature appears to shift to slightly higher temperatures when the particles decrease in size from 6 to 3 nm; however, the basic features remain the same.

To examine these desorption features more closely, we also measured TPD as a function of NO exposure, with the TPD curves for $^{15}N_2$ shown in Fig. 9. On the small particles, there was a shift to higher peak temperatures with decreasing initial coverage, consistent with a second-order desorption process, but there were otherwise no changes. For the large particles, all of the NO desorbed dissociatively at lower NO exposures. The N_2-desorption features were found to fill sequentially, with the 440-K peak filling only after the recombination peak had saturated. The sequential filling of the two N_2 peaks implies that the two features are not due to adsorption on different Rh particles.

The change in the desorption curves with particle size is probably very significant for understanding the structure sensitivity of NO reduction by CO on Rh catalysts. It has

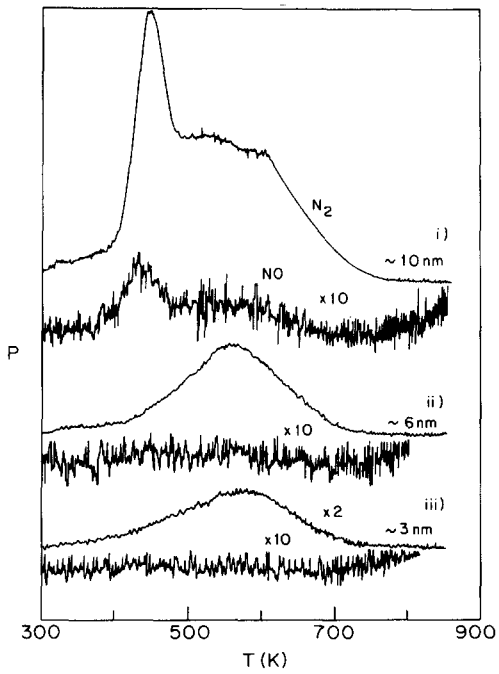

FIG. 8. TPD curves following a saturation exposure of NO from three different metal particle sizes of Rh on ZrO_2(100). Each sample was annealed to 800 K prior to NO exposure. The initial metal coverages were i) 5.7 × 10^{15}Rh/cm^2, ii) 1.0 × 10^{15}Rh/cm^2, and iii) 0.28 × 10^{15}Rh/cm^2.

been reported that Rh single crystals are much more active than Rh/Al_2O_3 (*3*), and that poorly dispersed catalysts are much more active on a surface area basis than highly dispersed catalysts (*10*). A model of the reaction between NO and CO has shown that elimination of the low-temperature, N_2 desorption process could significantly inhibit the overall reaction rate by covering the surface with dissociatively adsorbed nitrogen, which will block the adsorption of molecular NO and CO. Indeed, Auger spectra of a Rh(111) surface after reaction measurements showed high coverages of nitrogen (*3*) . At the same time, the TPD curves do not give any evidence that NO dissociation is inhibited on smaller Rh particles. NO dissociation was complete for all but the largest particles investigated.

We also examined NO adsorption on Rh films which had not been annealed, with the results shown in Fig. 10 for metal coverage of 5.7 ×10^{15}/cm^2 and 1.1 × 10^{15}/cm^2. For the lower Rh coverage, the shape of the TPD curve is unchanged by annealing. The only difference is that more $^{15}N_2$ left the surface prior to annealing. For the larger Rh coverage, rather broad $^{15}N_2$ and ^{15}NO peaks are observed with peak temperatures of ~500 K. There is no clear evidence of the feature due to NO_{ad} + N_{ad} at 440 K, which was observed for large particles after annealing. Although 5.7 × 10^{15}/cm^2 corresponds to more than 5 monolayers of Rh and the adsorption properties of a Rh film this thick would be expected to approach that of bulk Rh, this TPD curve does not look like those taken from large Rh particles or bulk Rh samples. The most likely explanation for the differences between the unannealed film and large particles of Rh is that the unannealed film contains sites which have a different coordination. From the film growth measurements, we know that the Rh film formed by deposition at 300 K is metastable. This film also exhibits a TPD curve for

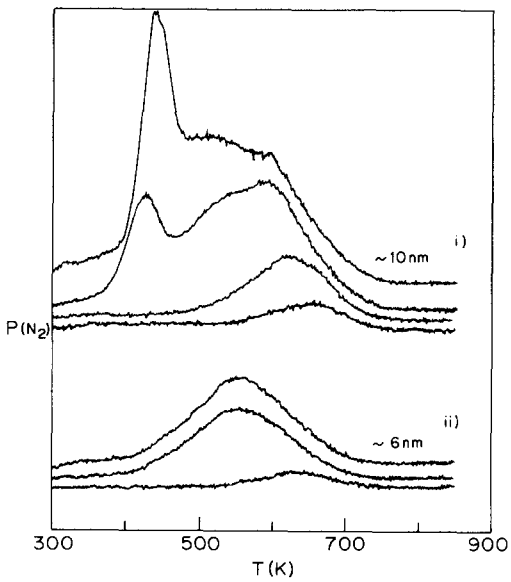

FIG. 9. N_2 TPD curves from Rh/ZrO_2(100) for varying initial NO coverages. The results indicate that the desorption features fill sequentially.

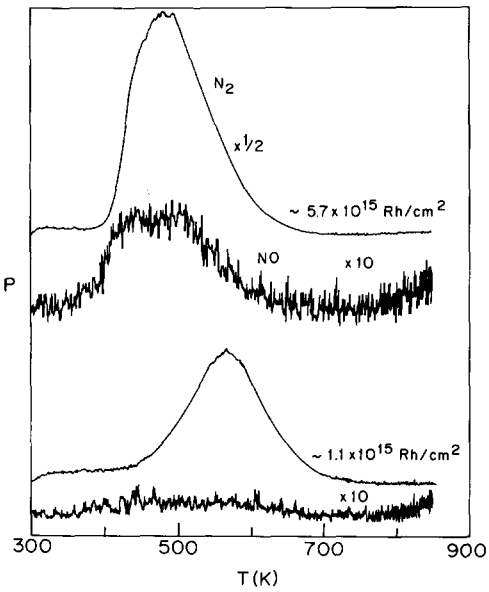

FIG. 10. TPD curves following NO adsorption on freshly deposited films of Rh on $ZrO_2(100)$.

NO which is more similar to that found on small Rh particles. This would again suggest that the results on smaller particles are due to morphological rather than support effects, and that the adsorption measurements on Rh do not provide evidence for strong support interactions on $ZrO_2(100)$.

DISCUSSION

The main conclusion we have reached from this study is that interactions between Rh and $ZrO_2(100)$ are relatively weak. Several observations point toward this. First, the growth of the Rh film is not expitaxial. While film growth is almost two dimensional, Rh forms a hexagonal overlayer on the cubic substrate and the Rh–Rh bond distance in the overlayer is close to the bulk value. The hexagonal orientation of the Rh layer indicates that there probably is an attractive interaction between Rh and ZrO_2, since this orientation maximizes the contact between the two phases. The enhanced thermal stability of Rh/ZrO_2 compared to Rh/Al_2O_3 catalysts also argues for attractive interactions between Rh and ZrO_2 (*2*); however, the Rh–Rh bonds must be stronger than the Rh–ZrO_2 bonds or else overlayer growth would be epitaxial. Second, desorption does not appear to be affected by the presence of ZrO_2. The TPD results for both CO and NO are very similar to those found for Rh on α-$Al_2O_3(0001)$, even for the smallest particles (*8, 9*). In particular, the TPD curves for CO from $Rh/ZrO_2(100)$ are very similar to measurements from bulk Rh surfaces. It does not appear that Rh has been chemically modified in any significant way by the proximity of ZrO_2.

It is of interest to compare previous results and conclusions for Pt on $ZrO_2(100)$ with those from this paper (*7*). In results similar to those for Rh, Pt formed overlayers which were nearly two-dimensional and hexagonal in orientation, with Pt–Pt bond distances close to that of bulk Pt. However, there were significant shifts in the desorption curves for CO from submonolayer Pt coverages on $ZrO_2(100)$ compared to CO from Pt on α-$Al_2O_3(0001)$ or oxidized Al (*9, 20*). On Al_2O_3, CO desorbed with a peak temperature near 510 K from small Pt particles, a temperature close to that found for highly stepped Pt surfaces, while the peak temperature was ~460 K for small Pt particles on $ZrO_2(100)$. It was suggested that the lower peak temperature for Pt on ZrO_2 is due to interactions between the Pt atoms and Zr^{+4} cations at the surface (*7*). This conclusion is now in question.

While it is certainly possible that Pt could interact with the Zr^{+4} cations more strongly than Rh does, it is also possible that the observations on Pt are due to morphological rather than chemical effects. Pt differs from Rh in that CO desorption is strongly affected by surface structure on Pt (*18*), while TPD curves for CO from various bulk Rh surfaces are virtually identical (*12–15*). Therefore, if ZrO_2 were to significantly affect the structure of the metal particles, one might expect to see a change in the results for Pt but not for Rh. Since there is an indication of attractive interactions between both metals the ZrO_2 substrate, morphological differ-

ences between metal particles on ZrO_2 and Al_2O_3 appear likely, especially for very small particles which would probably have the best contact with the oxide surface.

It is possible to explain changes in catalytic activity as being due to structural effects. While CO desorption on Rh is not structure sensitive, alkane hydrogenolysis has been shown to depend on particle size (*21*) and crystal orientation (*22*). NO reduction by CO over Rh also appears to be structure sensitive, with specific rates reported to increase by almost two orders-of-magnitude when the catalyst goes from 100% to <10% dispersion (*10*). In our TPD results, we observed significant changes in the N_2 desorption features with particle size. The desorption of N_2 due to $NO_{ad} + N_{ad} = N_2 + O_{ad}$ was only observed on the larger particles, and there appears to have been a slight decrease in the peak temperature of the recombination, N_2-desorption peak with increasing particle size. Calculations (*3, 8, 10*) and post-reaction AES measurements (*3*) have indicated that, under reaction conditions, the Rh surface is covered with N atoms which passivate the surface. Clearly, changes in the desorption rate of N_2 could strongly affect the surface coverage of N atoms and, therefore, reaction rates.

The changes in the activity of Rh catalysts with support are not as dramatic as changes observed with particle size. Therefore, differences in the N_2 desorption kinetics for Rh particles on different supports may be subtle. A comparison of the TPD curves for NO from $Rh/\alpha\text{-}Al_2O_3(0001)$ (*8*) and $Rh/ZrO_2(100)$ seems to indicate that differences exist. The feature due to $NO_{ad} + N_{ad} = N_2 + O_{ad}$ appeared at a smaller particle size on $Rh/\alpha\text{-}Al_2O_3(0001)$, which may be indicative of differences in the structure of the supported particles. Obviously, the idea that particle morphologies differ with support has yet to be definitively demonstrated. However, we believe it is likely that the origin of support effects may well be due to structural changes in the particles in certain systems, rather than electronic interactions, and that zirconia-supported metals may well be affected by this type of mechanism.

CONCLUSIONS

The interactions between Rh and ZrO_2 appear to be relatively weak. Rh films easily form particles upon heating, and even the smallest particles show adsorption properties which are similar to the properties of bulk metals. However, the interactions between Rh and ZrO_2 are capable of preferentially orienting the Rh particles. For reactions which are affected by particle size or crystallographic orientation, such as NO reduction by CO, orientation of the supported particles may provide the mechanism for support interactions.

ACKNOWLEDGMENTS

This work was supported by the DOE, Basic Energy Sciences, Grant DE-FG03-85-13350. Support for the electron microscopy experiments was partially provided by the NSF, MRL Program, Grant DMR 88-19885. We also thank Scott Roberts and Dave Luzzi for their technical assistance with the electron microscopy.

REFERENCES

1. Oh, S. H., *J. Catal.* **124,** 477 (1990).
2. Yao, H. C., Stepien, H. K., and Gandhi, H. S., *J. Catal.* **61,** 547 (1980).
3. Oh, S. H., Fisher, G. B., Carpenter, J. E., and Goodman, D. W., *J. Catal.* **100,** 360 (1986).
4. Gorte, R. J., *J. Catal.* **75,** 164 (1982).
5. Demmin, R. A., and Gorte, R. J., *J. Catal.* **90,** 32 (1984).
6. Roberts, S., and Gorte, R. J., *J. Chem. Phys.* **93,** 5337 (1990).
7. Roberts, S., and Gorte, R. J., *J. Phys. Chem.*, **95,** 5600 (1991).
8. Altman, E. I., and Gorte, R. J., *J. Catal.* **113,** 185 (1988).
9. Altman, E. I., and Gorte, R. J., *Surf. Sci.* **195,** 392 (1988).
10. Oh, S. H., and Eickel, C. C., *J. Catal.* **128,** 526 (1991).
11. Davis, L. E., MacDonald, N. C., Palmberg, P. W., Riach, G. E., and Weber, R. E., Eds., "Handbook of Auger Electron Spectroscopy," 2nd. ed. p. 47. Physical Electronics Industries, Eden Praire, MN, 1976.
12. Root, T. W., Schmidt, L. D., and Fisher, G. B., *Surf. Sci.* **150,** 173 (1985).

13. Baird, R. J., Ku, R. C., and Wynblatt, P., *Surf. Sci.* **97,** 346 (1980).
14. Ko, C. S., and Gorte, R. J., *Surf. Sci.* **161,** 597 (1985).
15. Thiel, P. A., Williams, E. D., Yates, J. T., and Weinberg, W. H., *Surf. Sci.* **84,** 54 (1979).
16. Ho, P., and White, J. M., *Surf. Sci.* **137,** 103 (1984).
17. Villarrubia, J. S., and Ho, W., *J. Chem. Phys.* **87,** 750 (1987).
18. McCabe, R. W., and Schmidt, L. D., *Surf. Sci.* **66,** 101 (1977).
19. Cavanagh, R. R., and Yates, J. T., *J. Chem. Phys.* **74,** 4150 (1981).
20. Altman, E. I., and Gorte, R. J., *Surf. Sci.* **172,** 71 (1986).
21. Yates, D. J. G., and Sinfelt, J. H., *J. Catal.* **8,** 348 (1967).
22. Datye, A. K., Hegarty, B. F., and Goodman, D. W., *Faraday Discuss. Chem. Soc.* **87,** 337 (1989).
23. Peden, C. H. F., Goodman, D. W., Blair, D. S., Berlowitz, P. J., Fisher, G. B., and Oh., S. H., *J. Phys. Chem.* **92,** 1563 (1988).